

The 2021 Mw7.0 Miyagi-Oki earthquake, northeastern Japan, nucleated from deep plate boundary: Implications for the initiation of the M9 earthquake cycle

Keisuke Yoshida¹, Toru Matsuzawa¹, and Naoki Uchida¹

¹Tohoku University

November 22, 2022

Abstract

Following the 2011 M9 Tohoku-Oki earthquake, the interplate seismicity drastically increased in the downdip extension; however, it disappeared within the rupture area. An Mw7.0 earthquake occurred in the downdip extension off Miyagi in March 2021, followed by an Mw6.7 earthquake in May 2021. To examine the initial evolution of the next M9 earthquake cycle, we examined the regional seismicity and source processes of the two M⁷ earthquakes. We found that the March Mw7.0 earthquake was nucleated at a conditionally stable patch where repeating earthquakes emerged after the Tohoku-Oki earthquake. The earthquake initiation from a conditionally stable patch at the deep plate boundary is probably a transient feature in the postseismic period of the previous M9 earthquake. The stress enhancement caused by the Mw7.0 event facilitated the subsequent May Mw6.7 earthquake. These two M⁷ earthquakes ruptured the western seismic patches of the 1978 Mw7.5 Miyagi-Oki earthquake, which is the most recent typical earthquake in an ~40-year interval of M^{7.5} earthquake sequence, and loaded the eastern shallow seismic patches for the sequence. Interplate seismicity in the updip area disappeared after the 2011 Tohoku-Oki earthquake. Assuming that the spatial pattern of interplate earthquakes will be restored to a situation similar to that before the Tohoku-Oki earthquake, the seismically active area should gradually expand to the updip area. Continued monitoring of interplate seismicity is essential to examine how plate-locking evolves during the M9 earthquake cycle.

Hosted file

essoar.10507585.1.docx available at <https://authorea.com/users/533568/articles/598242-the-2021-mw7-0-miyagi-oki-earthquake-northeastern-japan-nucleated-from-deep-plate-boundary-implications-for-the-initiation-of-the-m9-earthquake-cycle>

Hosted file

supple.docx available at <https://authorea.com/users/533568/articles/598242-the-2021-mw7-0-miyagi-oki-earthquake-northeastern-japan-nucleated-from-deep-plate-boundary-implications-for-the-initiation-of-the-m9-earthquake-cycle>

The 2021 Mw7.0 Miyagi-Oki earthquake, northeastern Japan, nucleated from deep plate boundary: Implications for the initiation of the M9 earthquake cycle

Keisuke Yoshida*, Toru Matsuzawa, Naoki Uchida

* Research Center for Prediction of Earthquakes and Volcanic Eruptions, Graduate School of Science, Tohoku University, Sendai, 980-8578, Japan

keisuke.yoshida.d7@tohoku.ac.jp

Key Points (< 140 words)

1. May 2021 Mw7.0 earthquake was initiated at a conditionally stable patch where repeating earthquakes emerged after the Tohoku-Oki earthquake
2. May 2021 Mw7.0 earthquake facilitated the March Mw6.7 earthquake in the south via changes in stress
3. These earthquakes increased strain energy in the updip area, including the area where ~M7.5 earthquakes have repeatedly occurred

Abstract (231 words)

Following the 2011 M9 Tohoku-Oki earthquake, the interplate seismicity drastically increased in the downdip extension; however, it disappeared within the rupture area. An Mw7.0 earthquake occurred in the downdip extension off Miyagi in March 2021, followed by an Mw6.7 earthquake in May 2021. To examine the initial evolution of the next M9 earthquake cycle, we examined the regional seismicity and source processes of the two M~7 earthquakes. We found that the March Mw7.0 earthquake was nucleated at a conditionally stable patch where repeating earthquakes emerged after the Tohoku-Oki earthquake. The earthquake initiation from a conditionally stable patch at the deep plate boundary is probably a transient feature in the postseismic period of the previous M9 earthquake. The stress enhancement caused by the Mw7.0 event facilitated the subsequent May Mw6.7 earthquake. These two M~7 earthquakes ruptured the western seismic patches of the 1978 Mw7.5 Miyagi-Oki earthquake, which is the most recent typical earthquake in an ~40-year interval of M~7.5 earthquake sequence, and loaded the eastern shallow seismic patches for the sequence. Interplate seismicity in the updip area disappeared after the 2011 Tohoku-Oki earthquake. Assuming that the spatial pattern of interplate earthquakes will be restored to a situation similar to that before the Tohoku-Oki earthquake, the seismically active area should gradually expand to the updip area. Continued monitoring of interplate seismicity is essential to examine how plate-locking evolves during the M9 earthquake cycle.

Plain Language Summary (199 words)

Following the 2011 M9 Tohoku-Oki earthquake, plate-boundary earthquakes stopped occurring within the rupture area, while many more earthquakes started

to occur in the downdip extension. An M7.0 earthquake occurred in the downdip extension off Miyagi in March 2021, followed by an M6.7 earthquake in May 2021. By examining these two plate-boundary earthquakes, we found that the first M7.0 earthquake was initiated in an abnormal area where earthquakes could not occur before the Tohoku-Oki earthquake. Earthquake initiation from such an area is possible only under intense after-effects of the previous M9 earthquake. The M7.0 earthquake increased the strain energy in the surrounding area and facilitated the subsequent May M6.7 earthquake. These two M~7 earthquakes ruptured the western part of the focal region of the 1978 M7.5 Miyagi-Oki earthquake, which is the most recent typical earthquake in an M~7.5 earthquake sequence at ~40-year intervals. These two earthquakes further increased the strain energy in the shallow eastern areas. Plate-boundary earthquakes are expected to restart in the Tohoku-Oki rupture area in the future. Thus, continued monitoring of plate-boundary earthquakes along the Japan Trench is crucial to reveal the after-effects of the 2011 M9 earthquake and the preparation process of the next M9 earthquake.

1. Introduction

M~7.5 earthquakes have occurred at intervals of about 40 years off Miyagi (Miyagi-Oki), northeastern Japan. These M~7.5 earthquakes ruptured multiple seismic patches with different combinations of the rupture patches. The 1978 Mw7.5 Miyagi-Oki earthquake is the most recent typical example (blue contour in Figure 1; Yamanaka & Kikuchi, 2004), which ruptured a region containing the focal areas of the 1933 M7.1, 1936 M7.4 (thin black contour in Figure 1), and 1937 M7.1 earthquakes (Umino et al., 2006, 2007). The 2005 Mw7.2 Miyagi-Oki earthquake ruptured the southeastern part of the rupture area of the 1978 earthquake (broken black contour in Figure 1; Yaginuma et al., 2006), but the other parts remained unruptured (Okada et al., 2005; Wu et al., 2008).

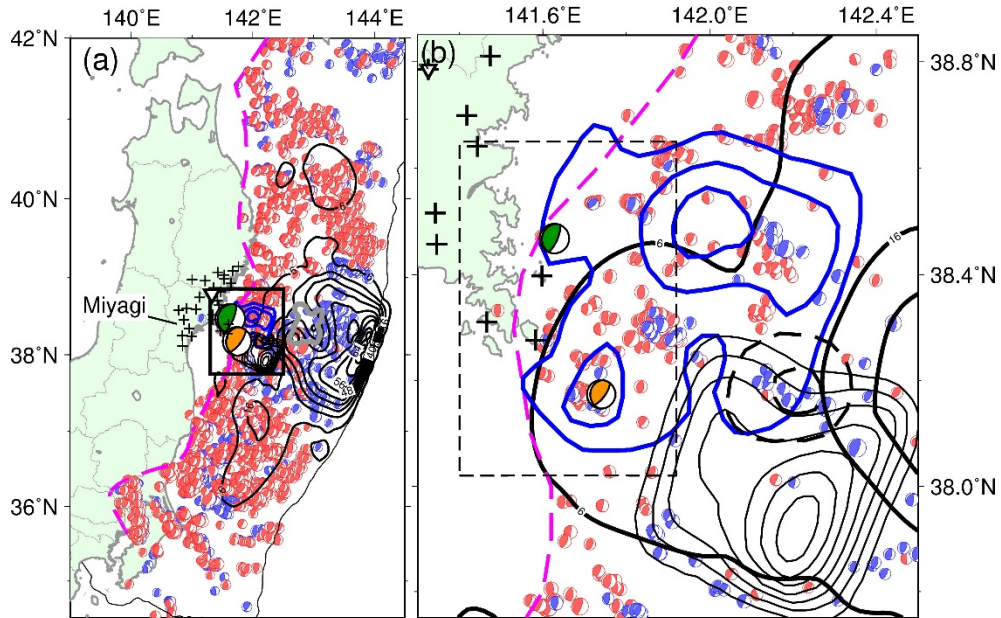


Figure 1. Interplate earthquakes from January 1, 1997, to May 14, 2021, selected by the method of Asano et al. (2011) from the F-net moment tensor catalog. Areas are (a): along the Japan Trench (black line) and (b): off Miyagi. Green and orange beach balls show the focal mechanisms of the March 2021 Mw7.0 and the May 2021 Mw6.7 Miyagi-Oki earthquakes, respectively. Light blue and light red beach balls show the focal mechanisms before and after the 2011 Tohoku-Oki earthquake, respectively. The thick black contour shows the coseismic slip distribution of the Tohoku-Oki earthquake (Inuma et al., 2012). The thin black, blue, gray, and black broken contours show the slip areas of the M7-7.5 earthquakes off Miyagi in 1936, 1978, 1981 (Yamanaka and Kikuchi, 2004), and 2005 (Yaginuma et al., 2006), respectively. The pink broken curve represents the downdip limit of interplate earthquakes (Igarashi et al., 2001; Uchida et al., 2009; Kita et al., 2010). The crosses show the stations used for hypocenter relocation in this study. The inverse triangle shows the station, the waveforms of which are shown in Figure 5.

The 2011 M9 Tohoku-Oki earthquake caused a large coseismic slip in a wide area along the Japan Trench, including the source area of the 1978 Mw7.5 Miyagi-Oki earthquake (e.g., Inuma et al., 2012), and perturbed the generations of the interplate earthquakes along the Japan trench. Interplate seismicity almost disappeared inside the rupture area of the Tohoku-Oki earthquake, while many interplate earthquakes followed the Tohoku-Oki earthquake in the surrounding area (e.g., Asano et al., 2011; Kato and Igarashi, 2012; Hasegawa & Yoshida, 2015; Nakamura et al., 2016). The coseismic and postseismic slips of the Tohoku-Oki earthquake increased the shear stress in the surrounding area (Asano et al., 2011; Ozawa et al., 2012; Hasegawa et al., 2012; Kato & Igarashi, 2012; Uchida

& Matsuzawa, 2013). The behavior of the repeating earthquakes changed after the Tohoku-Oki earthquake (Uchida et al., 2015); the magnitudes and rupture areas of many repeating earthquakes increased immediately after the Tohoku-Oki earthquake and gradually returned to normal. Furthermore, new repeating earthquake sequences emerged in some areas (Hatakeyama et al., 2017).

A decade after the 2011 Tohoku-Oki earthquake, an Mw7.0 ($M_{\text{JMA}}6.9$) earthquake occurred off Miyagi (Miyagi-Oki) on March 20, 2021, near the western edge of the rupture area of the 1978 Miyagi-Oki earthquake, which was followed by an Mw6.7 ($M_{\text{JMA}}6.8$) earthquake on May 1, 2021 (Figure 1). The low-angle reverse fault focal mechanisms and depths (~60 km) indicate that these earthquakes occurred on the plate boundary. These earthquakes were the first M~7 interplate earthquakes in the Miyagi-Oki area after the Tohoku-Oki earthquake.

The Tohoku-Oki earthquake provides a rare opportunity to investigate how the earthquake cycle of a great (M9) earthquake impacts the generation of smaller (M7-8) earthquakes on the same fault. The present study addresses this issue by examining the March 2021 Mw7.0 earthquake and the May 2021 Mw6.7 earthquake, which offer observations on the initial evolution of the M9 earthquake cycle. We define the earthquake cycle's initiation and end as immediately after the previous earthquake and immediately before the next M9 earthquake, respectively. We show that the March Mw7.0 mainshock was initiated in a deep plate boundary area, where the accumulated stress had been released aseismically before the Tohoku-Oki earthquake. We also show that the two M~7 Miyagi-Oki earthquakes and other smaller earthquakes contributed to reloading the M9 rupture area, including the main rupture area of the 1978 Mw7.5 Miyagi-Oki earthquake.

2. Method

2.1. Hypocenter relocation

We relocated earthquake hypocenters around the source regions of the 2021 Mw7.0 and Mw6.7 Miyagi-Oki mainshocks by following Yoshida and Hasegawa (2018a and b). The waveform cross-correlation-based double-difference earthquake relocation method (Waldhauser & Ellsworth, 2000) was applied to 5426 $M_{\text{JMA}} \geq 2$ earthquakes from March 1, 2003, to May 14, 2021, in the JMA (Japan Meteorological Agency) unified catalog (Figure S1). We assumed the 1-D velocity model by Ueno et al. (2002).

We used 49070 P-wave and 47566 S-wave differential arrival time data from the JMA unified catalog and 175817 P-wave and 204395 S-wave differential arrival time data derived from the waveforms. We computed the cross-correlation functions of band-passed waveforms (2-5 Hz) of nearby (< 3 km) earthquake pairs separately for P- and S-wave windows, starting 0.3s before their arrival and ending in 2.8 and 4.3s, respectively. The differential arrival time data were used if the cross-correlation coefficients were higher than 0.8. The P- and S-wave arrival times used to determine the P- and S-wave cross-correlation windows were obtained from the JMA unified catalog. If the arrival time was unavail-

able, theoretical travel times were used to set the time windows. The waveform data were derived from onland stations (Figure 1) by Tohoku University, JMA, NIED (National Research Institute for Earth Science and Disaster Resilience). Two stations in small islands (Figure 1b) were operated by Tohoku University.

We evaluated the uncertainty in the relative hypocenter locations by recalculating the hypocenters 1000 times based on bootstrap resampling of differential arrival time data. We computed the difference between the maximum and minimum values at the 95% confidence interval of the hypocenter locations to measure the estimation error.

2.2. Estimation of source processes

We first estimated the apparent moment rate functions (AMRFs) of the two mainshocks and inverted them to obtain the spatiotemporal distributions of the mainshock slips in the same manner as Yoshida et al. (2020), basically after Ross et al. (2018).

To estimate the AMRFs, we applied the iterative time-domain approach by Ligorria and Ammon (1999) after Kikuchi and Kanamori (1982) to the S-waves (transverse component) with a non-negative constraint. If the obtained AMRF could explain more than 80% of the observed waveforms in variance reduction, we regarded the deconvolution as ‘successful.’ We used the acceleration waveform data from onland stations of NIED KiK-net (NIED, 2019a) and offshore stations of S-net (offshore; NIED, 2019b). The orientations of the S-net sensors were corrected as per Takagi et al. (2019). The cut-off frequency of the low-pass (fourth-order Butterworth-type) filter used in the deconvolution was set to 0.35 Hz.

The AMRFs were inverted for the spatiotemporal distribution of slip on the fault, following Hartzell and Heaton (1983) and Mori and Hartzell (1990). We assumed that the source nucleated at the center of the fault model space, and the rupture front propagated over the fault with a constant velocity $V_r = 0.8 V_s$. The fault geometry was assumed to be rectangular with a fault strike of 190° and a dip angle of 25° , based on the focal mechanisms (Figure 1). The fault length and width were set to twice the rupture distance over 25s (90 km). The fault was divided into 25×25 subfaults.

At each subfault, we represented the local moment rate function as a superposition of five synthetic sub-moment rate functions (sMRFs). The first sMRF started when the rupture front reached the center of the subfault, and the four subsequent sMRFs followed at a regular interval t_h at each subfault. We obtained the amplitudes of the sMRFs by solving the following linear equation:

$$d_{\text{obs}} = Gm \quad (1)$$

where d_{obs} is the data vector containing the mainshock waveforms, G is the matrix of synthetics (AMRF waveforms), and m is the solution vector of the sMRF amplitudes. We computed the relative delay times between each subfault and station using the 1-D model of Ueno et al. (2002). We introduced a constant

damping factor (λ) and a smoothing factor (e_s) with the same value ($\lambda = e_s = 2$), which was determined based on the trade-off curve (Figure S2) and employed the non-negative least-squares algorithm of Lawson and Hanson (1995). We assumed $t_h = 0.8$ s because of the minimum misfits for the two mainshocks. The rigidity was assumed to be 50 GPa to compute the slip rate from the moment rate. The total moment release of the subfaults was multiplied by the constant to match the seismic moment of the earthquake.

We used the variance reduction VR between the theoretical and observed AMRFs to measure the consistency.

$$VR(\%) = 100 \times \sum_{i=1}^n \left(1 - \frac{\sum (d_i(t_j) - s_i(t_j))^2}{\sum d_i^2(t_j)} \right) \quad (2)$$

where $d_i(t_j)$ and $s_i(t_j)$ are the observed and synthetic time series of the i -th AMRFs, respectively, and n is the number of the AMRFs. We evaluated the uncertainty in the coseismic slip distribution by recalculating it 1000 times based on bootstrap resampling of the AMRF data.

3. Results

3.1. Seismicity around the focal regions

We obtained the relocated hypocenters of 5298 events (Figure 2). The medians of the uncertainties in the hypocenters are 0.003° (0.26 km) in longitude, 0.002° (0.21 km) in latitude, and 0.28 km in depth. The across-strike cross-section of the relocated hypocenters (Figure 2) shows that not only interplate earthquakes but also intraslab and intraplate earthquakes occurred in this region. We regarded the 2736 earthquakes within 3 km of the plate boundary (Hasegawa et al., 1994) as interplate earthquakes and hereafter focused on them (Figure 3).

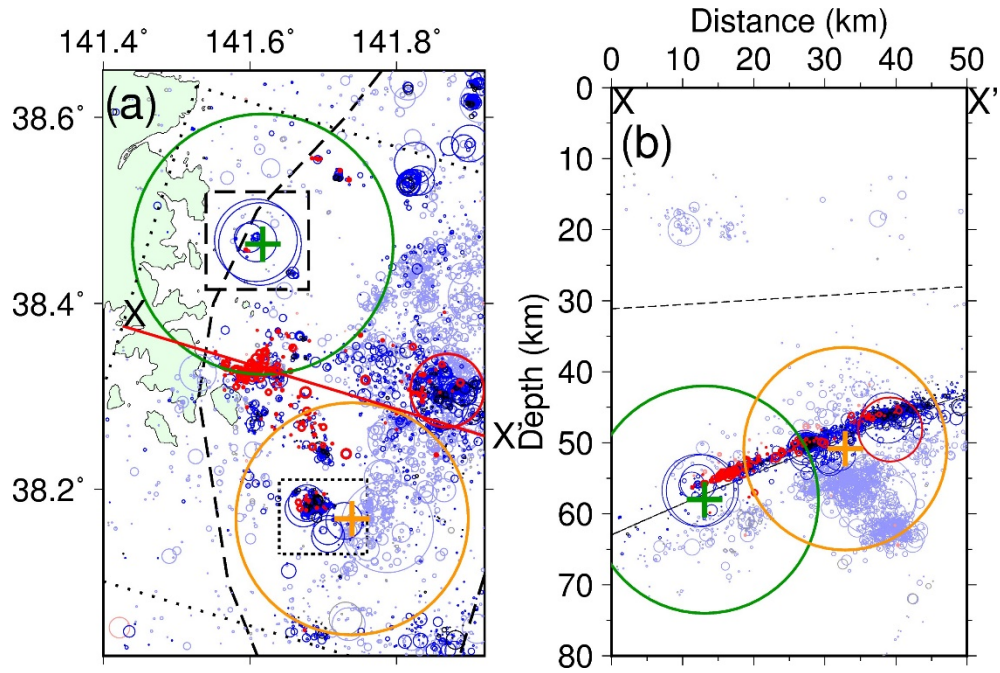


Figure 2. Seismicity around the March 2021 Mw7.0 and the May 2021 Mw6.7 earthquakes. (a): Map and (b): cross-section showing the relocated hypocenters (circles) with $M_{JMA} \geq 2$. Green and orange circles with crosses show the hypocenters of the March 2021 Mw7.0 and the May 2021 Mw6.7 Miyagi-Oki earthquakes, respectively, with the circle sizes indicating the rupture areas assuming a stress drop of 3 MPa. Blue circles show earthquakes that occurred between the Tohoku-Oki earthquake and the March 2021 Mw7.0 earthquake. Black and red ones show the earthquakes before the Tohoku-Oki earthquake and after the 2021 Mw7.0 earthquake, respectively. Circles with light color show the earthquakes more than 3 km away from the plate boundary (Hasegawa et al., 1994). The broken line denotes the Moho depth (Uchida et al., 2010).

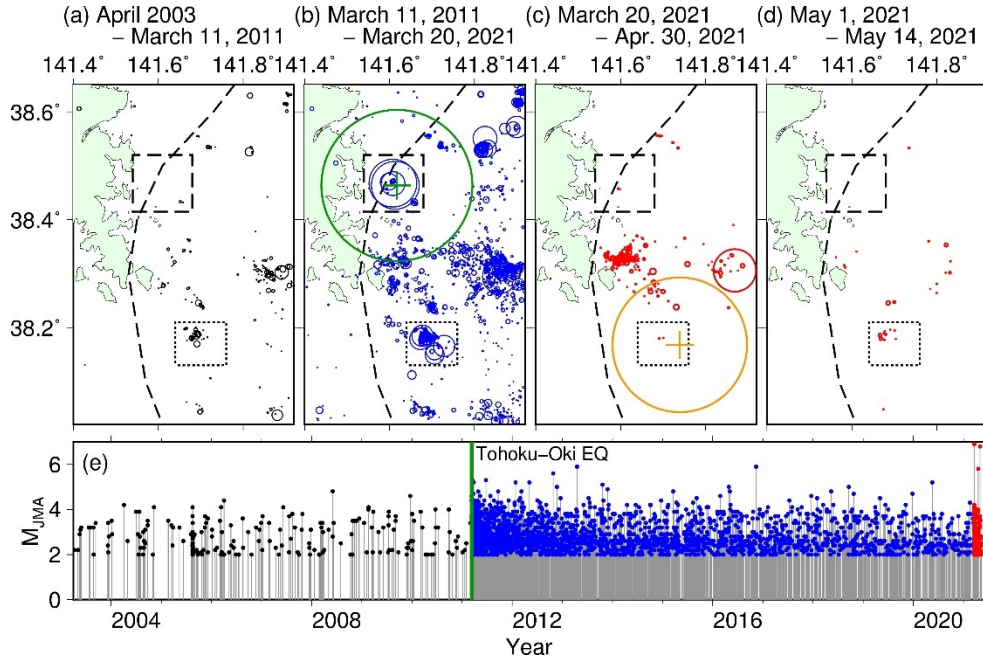


Figure 3. Interplate seismicity around the March 2021 Mw7.0 earthquake and the May 2021 Mw6.7 earthquake. (a): Before the 2011 Tohoku-Oki earthquake (April 2003 to March 11, 2011) (b): after the Tohoku-Oki earthquake and before the March 2021 Mw7.0 earthquake (March 11, 2011, to March 20, 2021), (c): after the March 2021 Mw7.0 earthquake and before the May 2021 Mw6.7 earthquake (March 20, 2021, to April 2021), and (d): after the May 2021 Mw6.7 earthquake (May 1, 2021, to May 13, 2021). The color of the circles indicates the occurrence times of the earthquakes, as in Figure 2. The circle sizes correspond to the source times of the earthquakes, as in Figure 2. The color of the circles indicates the occurrence times of the earthquakes, as in Figure 2. (e): Magnitude-Time (M-T) diagram.

A small number of interplate earthquakes occurred in the study area before the Tohoku-Oki earthquake, but the number sharply increased after the Tohoku-Oki earthquake (Figures 3e and 4). The increase in seismicity was pronounced near the hypocenter of the March 2021 Mw 7.0 mainshock (the broken rectangle in Figures 2a and 3a–e). A magnified view (Figure 4) shows that four M5–6 earthquakes (broken circles) occurred very close to the mainshock hypocenter: an Mw5.3 earthquake in 2011, an Mw5.9 earthquake in 2013, an Mw6.1 earthquake in 2016, and an Mw5.1 earthquake in 2018. The inter-event distances of these four earthquakes were much shorter than the source sizes of the four earthquakes (circle size in Figure 4a) and the mainshock, even when considering the estimation error; they probably ruptured the same seismic patch. Inside the M5–6 repeating earthquake source regions, M2–3 repeating earthquakes also occurred (Figures 4a and b), forming a hierarchical structure. Few earthquakes occurred around this region before the Tohoku-Oki earthquake (Figure 4c); almost all

of these repeating earthquakes occurred after the Tohoku-Oki earthquake. The March 2021 Mw7.0 mainshock rupture (green star in Figure 4) initiated near the M5-6 repeating earthquake sequence and the M2-3 repeating earthquake sequences.

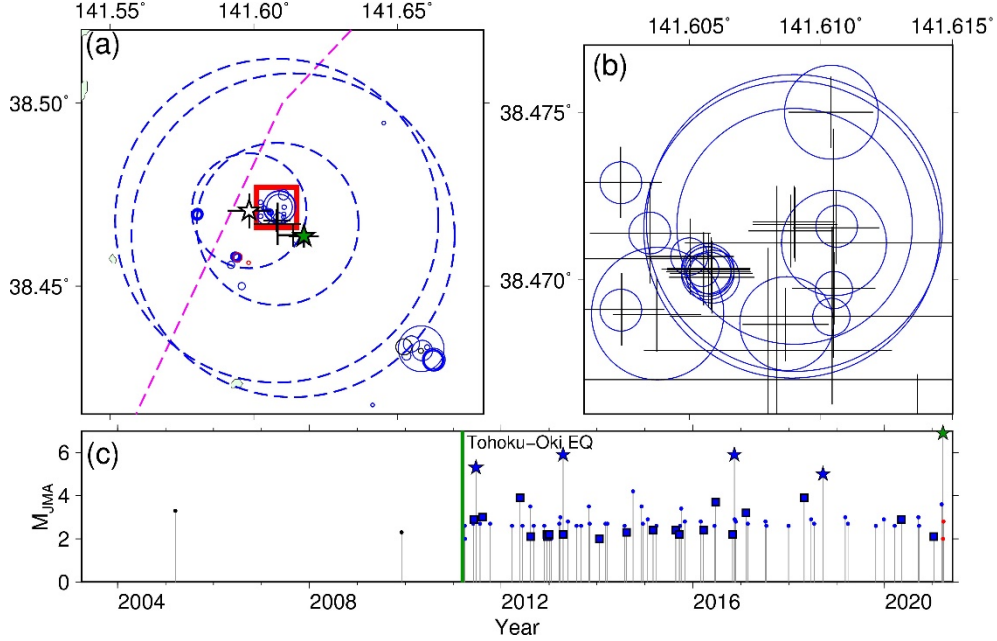


Figure 4. Seismicity near the hypocenter of the March 2021 Mw7.0 mainshock (green star). (a) and (b): relocated hypocenters in the areas indicated by the red rectangle in Figures 3 and 4a, respectively. Broken circles indicate the four M5-6 repeating earthquakes. The vertical and horizontal lines show the 95 % confidence intervals of the hypocenters. (a) shows the confidence intervals only for $M > 5$ earthquakes, while (b) for all earthquakes. The white star shows the event (EGF event) whose waveforms were used for the empirical Green’s functions (EGFs). (c): M-T diagram. Blue stars indicate the four M5-6 repeating earthquakes, squares show the events in the range of (b), and circles show other events in the range of (a). The events are represented in the same colors as those in Figure 2.

Figure 5 compares the initial parts of the acceleration waveforms of the March Mw7.0 mainshock (bottom) and the M5-6 repeating earthquakes observed at a nearby station (MYGH04: triangle in Figure 1a, b). They have similar shapes near the onsets ($t=0-1$ s) despite the waveforms containing high frequencies ($f > 1$ Hz) that are affected by their rupture processes. The initial waveform ($t=0-1$ s) of the Mw7.0 mainshock is especially similar to the 2013 Mw5.9 earthquake, 2016 Mw6.1 earthquake, and 2018 Mw5.1 earthquake (Figures 5d, g, j, m), suggesting that their initial ruptures evolved similarly. The waveform amplitude of the Mw7.0 mainshock is smaller than that of the 2013 Mw5.9 earthquake initially (t

< 1 s; Figure 5f), but becomes much larger at $t > 3$ s, reflecting the main rupture (Figures 5e, n). The wave amplitude of the Mw 7.0 earthquake is similar to those of the 2016 Mw6.1 and 2018 Mw5.1 earthquakes at the beginning (Figures 5i, l, o).

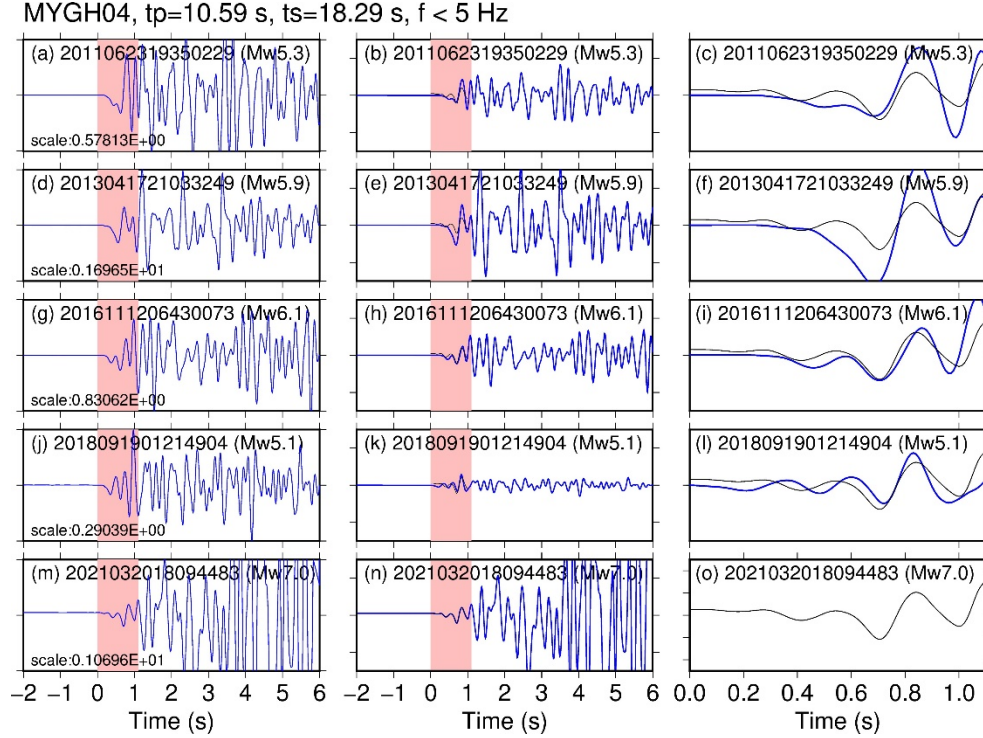


Figure 5. Low-passed acceleration waveforms ($f < 5$ Hz) of vertical P-wave of the 2021 Mw7.0 Miyagi-Oki earthquake and the nearby four M_{JMA} 5-6 earthquakes (shown by the broken circles in Figure 4a). The left panels (a, d, g, j, m) show the waveforms normalized by the maximum amplitudes during the first 2s. The middle ones (b, e, h, k, n) show the waveforms without normalization. The right ones (c, f, i, l, o) show the enlarged view of the initial waveforms (colored in the left and middle ones) without normalization. The black traces show the March mainshock.

The aftershocks of the March mainshock (Figure 3c) focused on the southern area from the mainshock hypocenter (green cross in Figure 3b). The May Mw6.7 mainshock occurred further to the south (orange cross in Figure 3c). Earthquakes occurred near the hypocenter of the May mainshock, even before the Tohoku-Oki earthquake (Figures 3a, S3). The number rapidly increased after the Tohoku-Oki earthquake, and a few earthquakes occurred after the March mainshock and before the May mainshock (Figure S3).

3.2. Rupture processes

We chose the waveforms of the 2018 Mw5.1 earthquake (Figures 5i, j, and white star in Figure 4) as the EGFs for the May Mw7.0 mainshock and the waveforms of the 2020 M5.2 earthquake (white star in Figure S3) for the March Mw6.7 mainshock because of their close distances. We derived 52 AMRFs for the March Mw7.0 mainshock and 62 AMRFs for the May Mw6.7 mainshock (Figures 6, 7) from approximately 200 observations.

The AMRFs of the two mainshocks showed a clear directional dependence. In the March Mw7.0 mainshock, the AMRFs had large amplitudes and short durations at western and southern stations, while they had two pulses with small amplitudes and long durations at northern stations (Figures 6a, 7a). This directional dependence suggests that the March mainshock comprised two major slips, the first rupture propagated in a southeastern direction, and the latter slip occurred south of the first one. In the May Mw6.7 mainshock, the AMRF amplitudes tended to be larger in the north and smaller in the south. The AMRF amplitudes were also smaller with longer durations at the western stations. This directional dependence suggests that the May mainshock propagated to the east and the north.

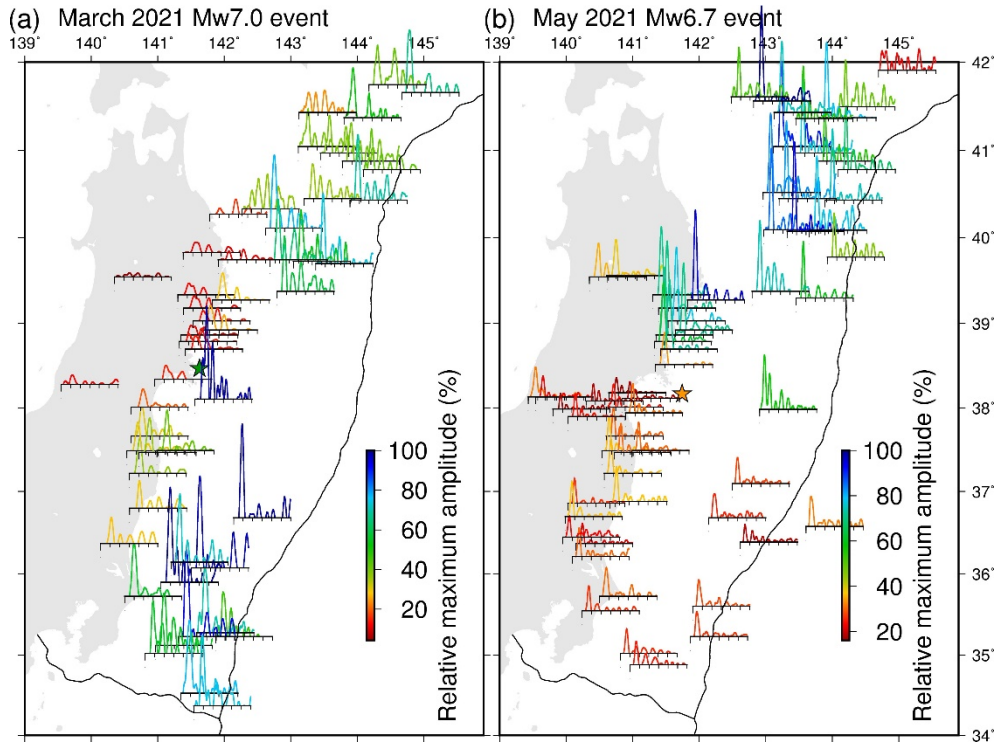


Figure 6. AMRFs of (a): the March 2021 Mw7.0 mainshock and (b): the May 2021 Mw6.7 mainshock. Their maximum amplitudes are presented based on the color scale. Tick marks denote 5s intervals. The stars show the corresponding earthquake epicenters.

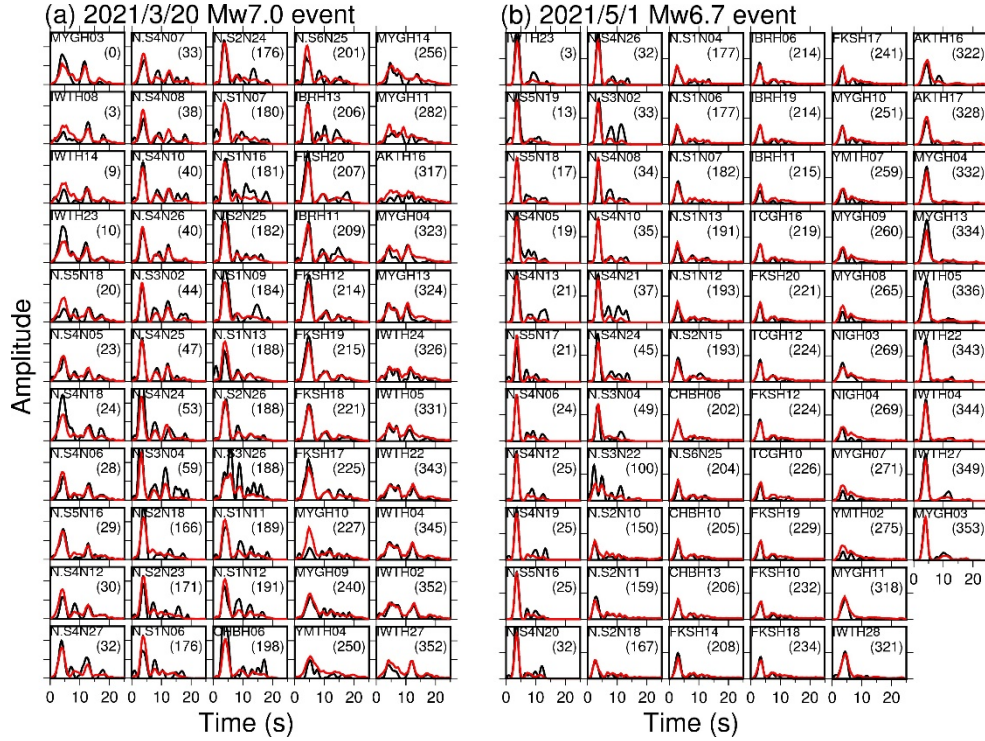


Figure 7. Observed AMRFs (black traces) compared with computed ones (red traces) for (a): the March 2021 Mw7.0 event and (b): the May 2020 Mw6.7 event. The numbers in parentheses indicate the respective azimuth angles of the stations.

The slip distributions obtained from the AMRF inversions (Figure 8) well reproduced the observed AMRFs (Figure 7) and are consistent with the above inferences from the AMRFs. The March Mw7.0 mainshock had two large slip regions: several km ESE (first rupture; $t=4-7$ s) and ~ 20 km south of the hypocenter (second rupture; $t=8-12$ s). In the May Mw6.7 mainshock, the maximum slip area was located a few kilometers southeast of the hypocenter. The total slip area was longer in the north direction as a moderate slip propagated to the north. The initial ruptures propagated in the updip direction for both earthquakes. These characteristics were robust among the results of bootstrap resampling (Figure S4) and did not change if different sizes of fault model space (Figure S5) or different rupture speeds (Figure S6) were assumed.

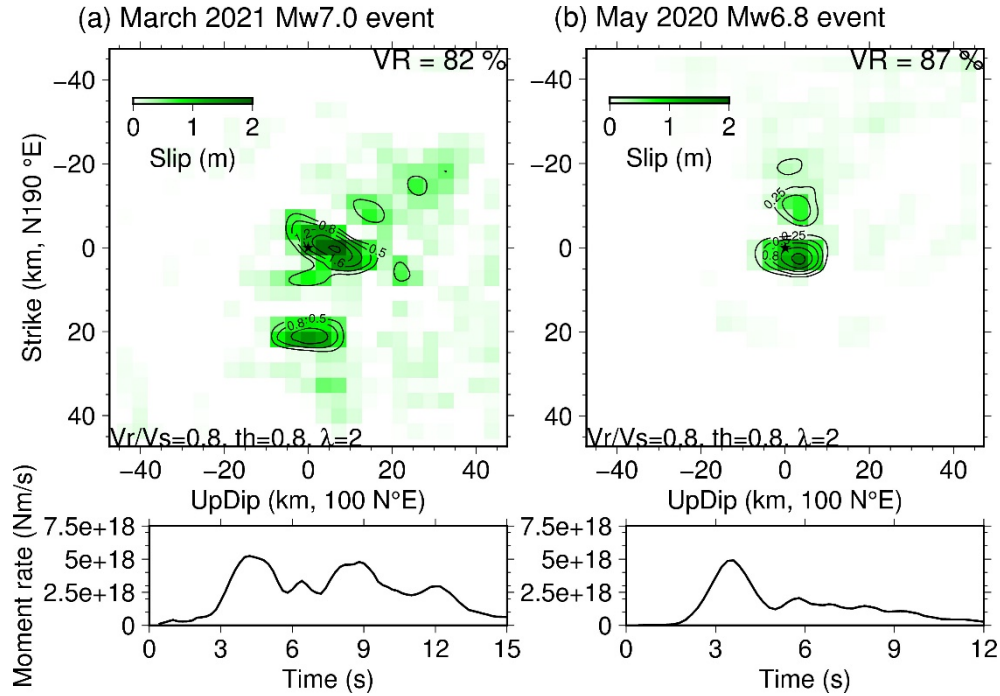


Figure 8. Results of the waveform inversions of (a): the March 2021 Mw7.0 event and (b): the May 2020 Mw6.7 event. The upper panels show the coseismic slip distributions, and the lower panels show the source time functions.

The rupture area of the March mainshock showed a complementary relationship with the aftershock distribution (Figure 9a). Most aftershocks were located just north of the southern patch at 38.3°N and 141.6°E . Figure 9c shows the shear stress change on the plate boundary due to the March mainshock slip based on Okada (1992) with Poisson’s ratio of 0.25 and rigidity of 50 GPa. Here, we discarded areas with non-significant slips (less than 0.3 m; Fig. S4) from the coseismic slips to avoid contamination from nonsignificant slips. The shear stress on the plate boundary should increase in areas far from the mainshocks (where no coseismic slip occurs) and in the aftershock area, regardless of this operation (Figure S7). The aftershocks and the May mainshock (orange star in Figures 9b, c) occurred in the region where the shear stress increased by the mainshock rupture (Figures 9c and S7).

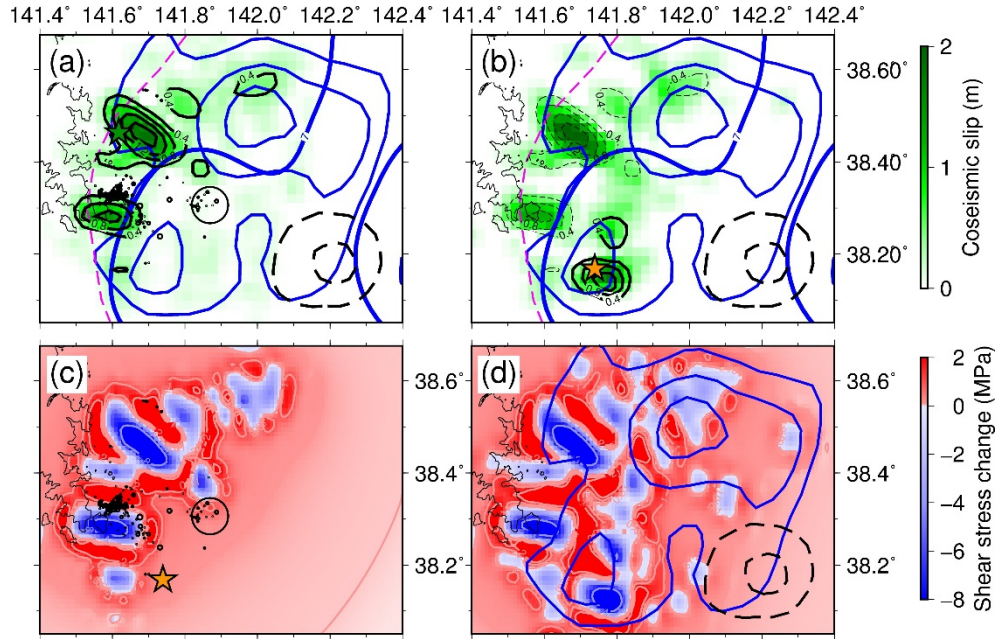


Figure 9. Relationship between the source regions of the 2021 Mw7.0 and Mw6.7 mainshocks and the 1978 and 2005 Miyagi-Oki earthquakes. The green and orange stars show the hypocenters of the March 2021 Mw7.0 earthquake and the May 2021 Mw6.7 earthquake, respectively. (a) and (b): Comparison of the coseismic slip distribution. The contours and the color scale indicate the coseismic slip distribution of the March mainshock in (a) and that of the sum of the two 2021 earthquakes in (b). (c): Shear stress change by the March 2021 Mw7.0 earthquake on the plate boundary. (d): Summed shear stress change by the two 2021 earthquakes on the plate boundary. The thick blue and thin black contours in (a) and (c) show the slip area of the 1978 Mw7.5 (Yamanaka & Kikuchi, 2004) and the 2005 Mw7.2 Miyagi-Oki earthquake (Yaginuma et al., 2006), respectively. Black circles in (a) and (c) show the relocated hypocenters of the earthquakes after the March 2021 Mw7.0 earthquake and before the May 2021 Mw6.7 earthquake.

The energy-based stress drop, calculated as the weighted mean of the shear stress change with respect to the slip amount (Noda et al., 2013), was 3.3 MPa for the March Mw7.0 mainshock and 1.8 MPa for the May Mw6.7 mainshock. The estimates of the average stress drops can vary by several times when assuming different model space lengths, even when using the weighted average. The average stress drops of the March Mw7.0 mainshock and the May Mw6.7 earthquake are 10.5 and 2.8 MPa, respectively, in the small model space case (Figs. S5a and c). The average value in the large model space case is 1.2 and 0.4 MPa for the March Mw7.0 mainshock and May Mw6.7 earthquake, respectively (Figs. S5c and d). The primary reason for this difference is that, in a larger

model space case, small artificial slips are distributed over the fault, leading to underestimation of the weighted average of the stress drops. However, in the case of a smaller model space, the actual slip area outside the model space may disappear artificially. From here on, we used the results of the main models (Figure 8).

We estimated the radiation energy E_R using the method of Vassiliou and Kanamori (1982): $E_R = 5.2 \times 10^{14}$ J for the March Mw7.0 mainshock and $E_R = 2.3 \times 10^{14}$ J for the May Mw6.7 mainshock. The scaled energies E_R/M_0 were 1.3×10^{-5} and 1.2×10^{-5} for the March Mw7.0 mainshock and the May Mw6.7 mainshock, respectively. The radiation efficiencies (Kanamori & Rivera, 2006) were 0.66 for the March mainshock and 0.59 for the May mainshock, falling within the typical range of Mw > 6.7 interplate earthquakes (Venkataraman & Kanamori, 2004).

4. Discussion

1. Generations of the March 2021 Mw7.0 earthquake and the May Mw6.7 earthquake

The March 2021 Mw7.0 mainshock was initiated in an area where repeating earthquakes emerged after the Tohoku-Oki earthquake. In this area, the seismicity rate of interplate events was quite low before the Tohoku-Oki earthquake. The focal depth of the March mainshock was near the lower limit of the interplate earthquakes (Figure 1; Igarashi et al., 2001), suggesting that aseismic slip was dominant in this area before the Tohoku-Oki earthquake when the creeping rate was close to or slower than the plate convergence rate. After the Tohoku-Oki earthquake, seismic slips started to occur in some of the aseismic segments (Uchida et al., 2015; Hatakeyama et al., 2017). This behavior suggests that the slip behavior in regions where interplate earthquakes emerged after the Tohoku-Oki earthquake depends on the loading rate, known as the conditionally stable region (Scholtz, 1998) — aseismic slip occurs under slow loading, but seismic slip can occur under faster loading (Uchida et al., 2015; Hatakeyama et al., 2017). The present observation suggests that the March mainshock was initiated in a conditionally stable region where the repeating earthquake sequence emerged after the Tohoku-Oki earthquake.

The temporarily increased magnitudes of repeating earthquakes in the downdip extension after the Tohoku-Oki earthquake tended to gradually decrease, probably because of the decay of the afterslip speed (Uchida et al., 2015). As for the M5-6 repeating earthquakes near the March mainshock hypocenter, the latest 2018 earthquake (Mw5.1) was smaller than the previous ones (Mw5.3-6.1) that occurred in 2011, 2013, and 2016 (Figure 4c). The onset amplitude of the March mainshock waveform was also smaller than that of the 2013 earthquake and comparable to that of the 2016 and 2018 earthquakes (Figure 5). However, the March mainshock became considerably larger than the previous M5-6 repeating earthquakes, as it involved the two large slip areas in the ESE and further south (Figure 8a). The previous M5-6 earthquakes did not cause large

slips in these distant areas.

The question to be considered is: why did only the earthquake in 2021 cause significant slips at the two distant patches? One possibility is the gradual accumulation of strain energy caused by the afterslip of the Tohoku-Oki earthquake; the stress level at the two large slip areas may have almost reached the fault strength only recently (after the 2018 Mw5.1 earthquake). The maximum coseismic slip amount is approximately a few meters, comparable to the afterslip amount derived from the GPS data (Iinuma et al., 2016; Tomita et al., 2020). This hypothesis may explain why only the earthquake in 2021 caused large slips in the two patches.

M2-3 repeating earthquakes occurred inside the source regions of the M5-6 repeating earthquakes near the mainshock hypocenter (Figure 4), suggesting that seismic patches in this region form a hierarchical structure similar to that formed by the Kamaishi repeating earthquakes and others (Uchida et al., 2007; Okuda & Ide, 2018; Ide, 2019). The ruptures of the M5-6 earthquakes and the March mainshock may have been initiated from a small patch (Ide & Aochi, 2005). The similar onsets of the March mainshock and the M5-6 earthquakes (Figure 5) may reflect that they grew similarly, suggesting that their rupture initiation and growth were influenced by persistent structure (Okuda & Ide, 2018; Ide, 2019). However, seismic slips in the source areas of the M5-6 repeating earthquakes and the initiation point of the March mainshock occurred only under fast loading, as in the postseismic phase of the 2011 M9 earthquake (i.e., the initial phase of the next M9 earthquake). The rupture behavior varies depending on the time-variant friction, stress, and loading conditions in the surrounding area.

The March mainshock increased the shear stress around the source region, explaining the aftershock cluster on the southern side (Figure 9b). The locations of aftershocks are limited, which is consistent with the hypothesis that the surrounding interplate segments are basically aseismic. The static stress change caused by the March mainshock also increased the shear stress near the May Mw6.7 mainshock in the southeast, which probably contributed to the occurrence of the May earthquake.

1. Evolution of plate-locking during the M9 earthquake cycle

Before the Tohoku-Oki earthquake, large interplate earthquakes occurred inside the main rupture area of the Tohoku-Oki earthquake (Figure 10). The M7.0, M6.9, and M7.3 earthquakes in 1981, 2003, and on March 9, 2011, respectively, occurred approximately 100 km east of the high seismicity areas at present. Repeating earthquakes and two other M~7 earthquakes have occurred since 1915 in offshore areas (Uchida and Burgmann, 2021). Geodetic data also show decadal unfastening of the plate boundary offshore of Miyagi and Fukushima before the earthquake (Mavrommatis et al., 2015; Yokota & Koketsu, 2015). An important factor for seismicity inside the rupture area of the Tohoku-Oki earthquake is fault creep, which may have intruded the main rupture area of the Tohoku-Oki earthquake during the later part of the earthquake cycle (e.g.,

Johnson et al., 2016), as inferred from the earthquake cycle simulations based on friction laws (e.g., Hori & Miyazaki, 2011; Nakata et al., 2016; Barbot, 2020). Therefore, fault creep may have modulated the shear stress inside the rupture area of the Tohoku-Oki earthquake and facilitated the inner interplate earthquakes before the Tohoku-Oki earthquake.

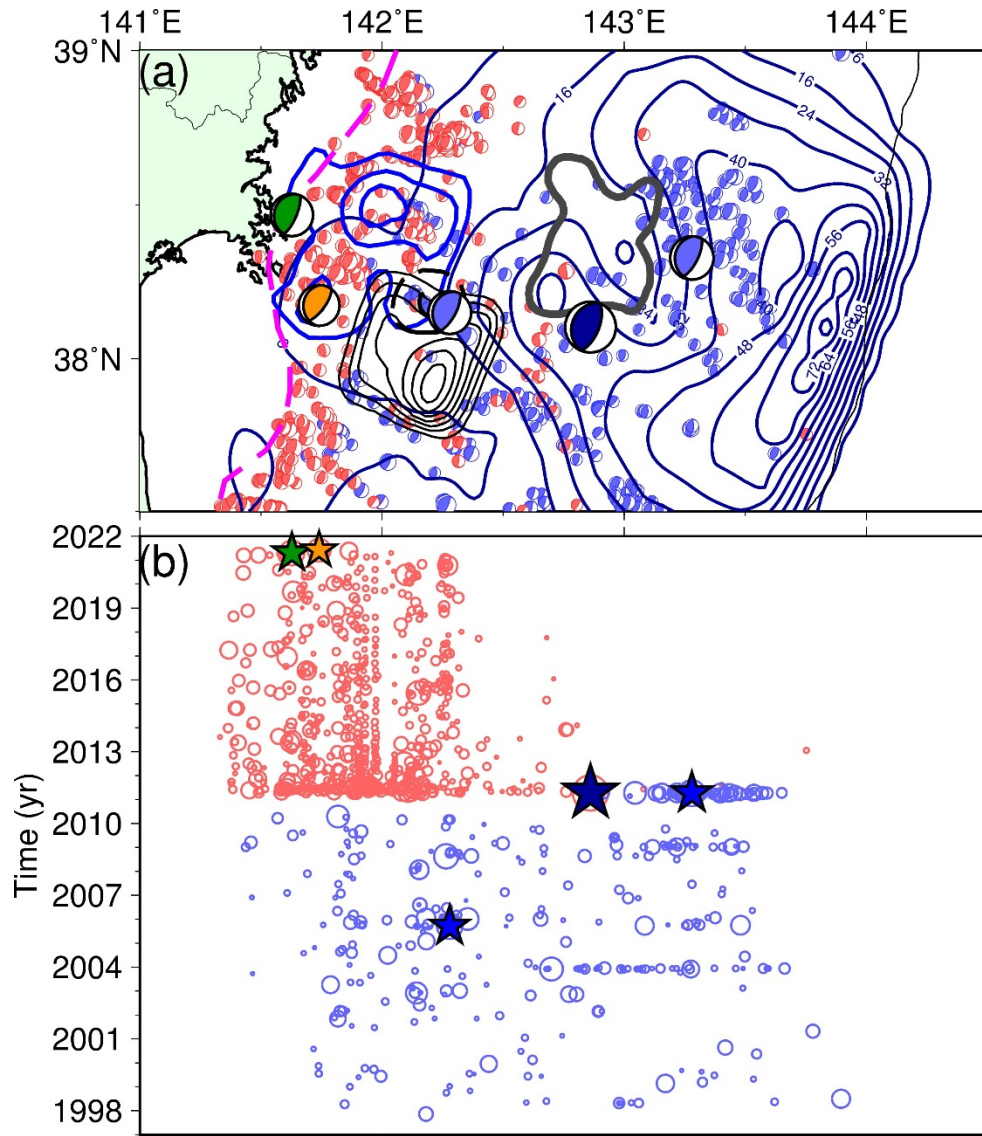


Figure 10. Interplate earthquakes before and after the Tohoku-Oki earthquake. (a) Map view. Green and orange beach balls show the focal mechanisms of the March 2021 Mw7.0 and the May 2021 Mw6.7 Miyagi-Oki earthquakes, respectively. Light blue and light red beach balls show the focal mechanisms before

and after the 2011 Tohoku-Oki earthquake, respectively. The large light blue beach ball indicates the largest M7.3 foreshock of the Tohoku-Oki earthquake on March 9, 2011. The blue, thin black, gray, and thick black contours show the slip areas of the M7-7.5 earthquakes off Miyagi in 1936, 1978, 1981 (Yamanaka and Kikuchi, 2004), and 2005 (Yaginuma et al., 2006), respectively. Other details are the same as in Figure 1. (b): latitude vs. occurrence time plot for interplate earthquakes before (blue) and after (red) the Tohoku-Oki earthquake.

After the Tohoku-Oki earthquake, postseismic slip occurred at the downdip extension of the rupture area (Ozawa et al., 2012; Uchida and Matsuzawa, 2013) instead of inner fault creep. Yoshida et al. (2021) found that the ruptures of the interplate earthquakes in the downdip area tended to propagate in the updip direction after the Tohoku-Oki earthquake. The fault creep (postseismic slip) near the downdip limit of the interplate earthquake (outside of the main rupture area of the Tohoku-Oki earthquake) probably facilitates the updip ruptures of current interplate earthquakes in the area. In the cases of the March 2021 Mw7.0 and May 2021 Mw6.7 mainshocks, the ruptures initially propagated in the updip direction. The March Mw7.0 and the May Mw6.7 mainshocks ruptured the western part of the rupture area of the 1978 Mw7.5 Miyagi-Oki earthquake (Seno et al., 1980; Yamanaka & Kikuchi, 2004). They increased the shear stress on the main rupture area of the 1978 earthquake, which is located further east.

The repeating earthquake occurrence at the patch estimated to be the initial rupture point of the March 2021 earthquake is considered a transient feature, which is possible only under the fast loading by the postseismic slip of the Tohoku-Oki earthquake. The nucleation of an M~7 earthquake from such a repeating earthquake patch is a also transient feature only in the initial phase of the M9 earthquake cycle. The present observation shows that the downdip extension of the Tohoku-Oki earthquake, showing aseismic to seismic transition after the earthquake, can produce not only small to moderate repeating earthquakes but also M~7 earthquakes. Because of their close distance to the land area, deep interplate events can cause stronger shaking on land than similar-sized offshore events. It is possible that the Miyagi-Oki seismic patches, which had caused M~7.5 earthquakes in about a 40-year interval, can simultaneously slip with the deep slip area and result in a larger earthquake. Therefore, it is extremely important to continue monitoring seismicity in this area to understand the spatiotemporal evolution of deep-interplate-earthquake ruptures.

Interplate seismicity in the updip area disappeared after the 2011 Tohoku-Oki earthquake (Figure 10). However, the spatial pattern of the interplate earthquakes will probably be restored to a situation similar to that before the Tohoku-Oki earthquake in the earthquake cycle of the next Tohoku-Oki earthquake. The seismically active area of the interplate earthquakes is expected to gradually expand to the updip area with continuing updip ruptures and creep intrusion. It is important to reveal how interseismic plate-relocking evolves and interplate earthquakes restart to occur inside the M9 Tohoku-Oki rupture area.

1. Conclusion

The 2011 Tohoku-Oki earthquake largely affected the stress and locking states on the plate boundary. Many earthquakes started to occur at downdip segments that were aseismic before the Tohoku-Oki earthquake, while interplate earthquakes almost disappeared inside the rupture area. The March 2021 Mw7.0 Miyagi-Oki earthquake was initiated from the previously aseismic segment in the downdip extension, where repeating earthquakes emerged after the Tohoku-Oki earthquake. The Mw7.0 earthquake propagated east and then south from the repeater patch, and the resultant shear stress redistribution facilitated the May 2021 Mw6.7 earthquake located about 30 km south. The Mw6.7 earthquake propagated east and then north. The two earthquakes ruptured the western part of the rupture area of the 1978 M7.5 Miyagi-Oki earthquake, which is a part of an earthquake sequence with an ~40-year cycle before the Tohoku-Oki earthquake. The two earthquakes increased the shear stress in the adjacent segment, including the main shallow rupture area of the 1978 earthquake.

Interplate earthquakes off Miyagi are currently concentrated in the downdip extension of the Tohoku-Oki earthquake. The spatial pattern of interplate seismicity is expected to be restored to a situation similar to that before the Tohoku-Oki earthquake in the future. The seismically active area expands to the updip area, affected by downdip earthquake ruptures and aseismic slips. Continued monitoring of interplate seismicity and aseismic slip at the deep plate boundary along the Japan Trench is crucial to reveal how the earthquake cycle evolves, leading to the next M9 earthquake.

Data Availability Statement

The results of the hypocenter relocation (Figure 2) and the slip distribution (Figure 8) are available in Datasets S1-S3. This study used hypocenters and arrival time data from the Japan Meteorological Agency (JMA) unified catalog (https://www.data.jma.go.jp/svd/eqev/data/bulletin/hypo_e.html) and the centroid moment tensor from the F-net moment tensor catalog (<https://www.fnet.bosai.go.jp/event/dreger.php?LANG=en>). The seismograms were collected and stored by the JMA, national universities, and National Research Institute for Earth Science and Disaster Resilience (NIED; <http://www.hinet.bosai.go.jp/?LANG=en>).

Acknowledgment

This research was supported by JSPS KAKENHI (grant number JP 20K14569). The figures were created using GMT (Wessel & Smith, 1998).

Reference

Asano, Y., Saito, T., Ito, Y., Shiomi, K., & Hirose, H. (2011). Spatial distribution and focal mechanisms of aftershocks of the 2011 off the Pacific coast of Tohoku Earthquake. *Earth, Planets and Space*, 63(7), 669–673.<https://doi.org/10.5047/eps.2011.06.016>

- Barbot, S. (2020). Frictional and structural controls of seismic super-cycles at the Japan trench. *Earth, Planets and Space*, 72(1). <https://doi.org/10.1186/s40623-020-01185-3>
- Hartzell, S. H., & Heaton, T. H. (1983). Inversion of strong ground motion and teleseismic waveform data for the fault rupture history of the 1979 Imperial Valley, California, earthquake. *Bulletin of the Seismological Society of America*, 73(6), 1553–1583. Retrieved from <http://www.bssaonline.org/content/73/6A/1553.short>
- Hasegawa, A., & Yoshida, K. (2015). Preceding seismic activity and slow slip events in the source area of the 2011 Mw 9.0 Tohoku-Oki earthquake: a review. *Geoscience Letters*, 2(1), 6. <https://doi.org/10.1186/s40562-015-0025-0>
- Hasegawa, A., Horiuchi, S., & Umino, N. (1994). Seismic structure of the north-eastern Japan convergent margin: A synthesis. *Journal of Geophysical Research: Solid Earth*, 99(B11), 22295–22311. <https://doi.org/doi:10.1029/93JB02797>
- Hasegawa, A., Yoshida, K., Asano, Y., Okada, T., Iinuma, T., & Ito, Y. (2012). Change in stress field after the 2011 great Tohoku-Oki earthquake. *Earth and Planetary Science Letters*, 355–356(null), 231–243. <https://doi.org/10.1016/j.epsl.2012.08.042>
- Hatakeyama, N., Uchida, N., Matsuzawa, T., & Nakamura, W. (2017). Emergence and disappearance of interplate repeating earthquakes following the 2011 M9.0 Tohoku-oki earthquake: Slip behavior transition between seismic and aseismic depending on the loading rate. *Journal of Geophysical Research: Solid Earth*, 122(7), 5160–5180. <https://doi.org/10.1002/2016JB013914>
- Hori, T., & Miyazaki, S. (2011). A possible mechanism of M 9 earthquake generation cycles in the area of repeating M 7.8 earthquakes surrounded by aseismic sliding. *Earth, Planets and Space*, 63(7), 773–777. <https://doi.org/10.5047/eps.2011.06.022>
- Ide, S. (2019). Frequent observations of identical onsets of large and small earthquakes. *Nature*, 573(7772), 112–116. <https://doi.org/10.1038/s41586-019-1508-5>
- Ide, S., & Aochi, H. (2005). Earthquakes as multiscale dynamic ruptures with heterogeneous fracture surface energy. *Journal of Geophysical Research: Solid Earth*, 110(11), 1–10. <https://doi.org/10.1029/2004JB003591>
- Igarashi, T., Matsuzawa, T., Umino, N., & Hasegawa, A. (2001). Spatial distribution of focal mechanisms for interplate and intraplate earthquakes associated with the subducting Pacific plate beneath the northeastern Japan arc: A triple-planed deep seismic zone. *Journal of Geophysical Research: Solid Earth*, 106(B2), 2177–2191. <https://doi.org/10.1029/2000jb900386>
- Iinuma, T., Hino, R., Kido, M., Inazu, D., Osada, Y., Ito, Y., et al. (2012). Coseismic slip distribution of the 2011 off the Pacific Coast of Tohoku Earth-

- quake (M9.0) refined by means of seafloor geodetic data. *Journal of Geophysical Research: Solid Earth*, 117(B7). <https://doi.org/10.1029/2012JB009186>
- Iinuma, T., Hino, R., Uchida, N., Nakamura, W., Kido, M., Osada, Y., & Miura, S. (2016). Seafloor observations indicate spatial separation of coseismic and postseismic slips in the 2011 Tohoku earthquake. *Nature Communications*, 7. <https://doi.org/10.1038/ncomms13506>
- Johnson, K. M., Mavrommatis, A., & Segall, P. (2016). Small interseismic asperities and widespread aseismic creep on the northern Japan subduction interface. *Geophysical Research Letters*, 43(1), 135–143. <https://doi.org/10.1002/2015GL066707>
- Kanamori, H., & Kikuchi, M. (1982). Inversion of complex body waves. *Bulletin of the Seismological Society of America*, 72(2), 491–506.
- Kanamori, H., & Rivera, L. (2006). Energy partitioning during an earthquake. In *Geophysical Monograph Series* (Vol. 170, pp. 3–13). <https://doi.org/10.1029/170GM03>
- Kato, A., & Igarashi, T. (2012). Regional extent of the large coseismic slip zone of the 2011 Mw 9.0 Tohoku-Oki earthquake delineated by on-fault aftershocks. *Geophysical Research Letters*, 39(15). <https://doi.org/10.1029/2012GL052220>
- Kita, S., Okada, T., Hasegawa, A., Nakajima, J., & Matsuzawa, T. (2010). Anomalous deepening of a seismic belt in the upper-plane of the double seismic zone in the Pacific slab beneath the Hokkaido corner: Possible evidence for thermal shielding caused by subducted forearc crust materials. *Earth and Planetary Science Letters*, 290(3–4), 415–426. <https://doi.org/10.1016/j.epsl.2009.12.038>
- Lawson, C. L., & Hanson, R. J. (1995). *Solving least squares problems*. SIAM.
- Ligorria, J. P., & Ammon, C. J. (1999). Iterative deconvolution and receiver-function estimation. *Bulletin of the Seismological Society of America*, 89(5), 1395–1400.
- Mavrommatis, A. P., Segall, P., Uchida, N., & Johnson, K. M. (2015). Long-term acceleration of aseismic slip preceding the Mw 9 Tohoku-oki earthquake: Constraints from repeating earthquakes. *Geophysical Research Letters*, 42(22), 9717–9725. <https://doi.org/10.1002/2015GL066069>
- Nakamura, W., Uchida, N., & Matsuzawa, T. (2016). Spatial distribution of the faulting types of small earthquakes around the 2011 Tohoku-oki earthquake: A comprehensive search using template events. *Journal of Geophysical Research: Solid Earth*, 121(4), 2591–2607. <https://doi.org/10.1002/2015JB012584>
- Nakata, R., Hori, T., Hyodo, M., & Ariyoshi, K. (2016). Possible scenarios for occurrence of M < 7 interplate earthquakes prior to and following the 2011 Tohoku-Oki earthquake based on numerical simulation. *Scientific Reports*, 6. <https://doi.org/10.1038/srep25704>

- NIED. (2019a). NIED K-NET, KiK-net, National Research Institute for Earth Science and Disaster Resilience. <https://doi.org/10.17598/NIED.0004>
- NIED. (2019b). NIED S-net, National Research Institute for Earth Science and Disaster Resilience. <https://doi.org/10.17598/NIED.0007>
- Noda, H., Lapusta, N., & Kanamori, H. (2013). Comparison of average stress drop measures for ruptures with heterogeneous stress change and implications for earthquake physics. *Geophysical Journal International*, *193*(3), 1691–1712. <https://doi.org/10.1093/gji/ggt074>
- Okada, T., Yaginuma, T., Umino, N., Kono, T., Matsuzawa, T., Kita, S., & Hasegawa, A. (2005). The 2005 M7.2 MIYAGI-OKI earthquake, NE Japan: Possible rerupturing of one of asperities that caused the previous M7.4 earthquake. *Geophysical Research Letters*, *32*(24), 1–4. <https://doi.org/10.1029/2005GL024613>
- Okuda, T., & Ide, S. (2018). Hierarchical rupture growth evidenced by the initial seismic waveforms. *Nature Communications*, *9*(1). <https://doi.org/10.1038/s41467-018-06168-3>
- Ozawa, S., Nishimura, T., Munekane, H., Suito, H., Kobayashi, T., Tobita, M., & Imakiire, T. (2012). Preceding, coseismic, and postseismic slips of the 2011 Tohoku earthquake, Japan. *Journal of Geophysical Research: Solid Earth*, *117*(B7), B07404. <https://doi.org/10.1029/2011JB009120>
- Ross, Z. E., Kanamori, H., & Hauksson, E. (2017). Anomalously large complete stress drop during the 2016 Mw5.2 Borrego Springs earthquake inferred by waveform modeling and near-source aftershock deficit. *Geophysical Research Letters*, *44*(12), 5994–6001. <https://doi.org/10.1002/2017GL073338>
- Seno, T., Shimazaki, K., Somerville, P., Sudo, K., & Eguchi, T. (1980). Rupture process of the Miyagi-Oki, Japan, earthquake of June 12, 1978. *Physics of the Earth and Planetary Interiors*, *23*(1), 39–61. [https://doi.org/10.1016/0031-9201\(80\)90081-3](https://doi.org/10.1016/0031-9201(80)90081-3)
- Takagi, R., Uchida, N., Nakayama, T., Azuma, R., Ishigami, A., Okada, T., et al. (2019). Estimation of the Orientations of the S-net Cabled Ocean-Bottom Sensors. *Seismological Research Letters*, *90*(6), 2175–2187. <https://doi.org/10.1785/0220190093>
- Tomita, F., Inuma, T., Ohta, Y., Hino, R., Kido, M., & Uchida, N. (2020). Improvement on spatial resolution of a coseismic slip distribution using postseismic geodetic data through a viscoelastic inversion. *Earth, Planets and Space*, *72*(1). <https://doi.org/10.1186/s40623-020-01207-0>
- Uchida, N., & Bürgmann, R. (2021). A Decade of Lessons Learned from the 2011 Tohoku-Oki Earthquake. *Reviews of Geophysics*, *59*(2). <https://doi.org/10.1029/2020rg000713>
- Uchida, N., Kirby, S. H., Okada, T., Hino, R., & Hasegawa, A. (2010).

Supraslab earthquake clusters above the subduction plate boundary offshore Sanriku, northeastern Japan: Seismogenesis in a graveyard of detached seamounts? *Journal of Geophysical Research: Solid Earth*, 115(B9), 1–13. <https://doi.org/10.1029/2009JB006797>

Uchida, N., & Matsuzawa, T. (2013). Pre- and postseismic slow slip surrounding the 2011 Tohoku-oki earthquake rupture. *Earth and Planetary Science Letters*, 374, 81–91. <https://doi.org/10.1016/j.epsl.2013.05.021>

Uchida, N., Matsuzawa, T., Ellsworth, W. L., Imanishi, K., Okada, T., & Hasegawa, A. (2007). Source parameters of a M4.8 and its accompanying repeating earthquakes off Kamaishi, NE Japan: Implications for the hierarchical structure of asperities and earthquake cycle. *Geophysical Research Letters*, 34(20). <https://doi.org/10.1029/2007GL031263>

Uchida, N., Nakajima, J., Hasegawa, A., & Matsuzawa, T. (2009). What controls interplate coupling?: Evidence for abrupt change in coupling across a border between two overlying plates in the NE Japan subduction zone. *Earth and Planetary Science Letters*, 283(1–4), 111–121. <https://doi.org/10.1016/j.epsl.2009.04.003>

Uchida, N., Shimamura, K., Matsuzawa, T., & Okada, T. (2015). Postseismic response of repeating earthquakes around the 2011 Tohoku-oki earthquake: Moment increases due to the fast loading rate. *Journal of Geophysical Research: Solid Earth*, 120(1), 259–274. <https://doi.org/10.1002/2013JB010933>

Ueno H, Hatakeyama S, Aketagawa T, Funasaki J, H. N. (2002). Improvement of hypocenter determination procedures in the Japan Meteorological Agency (in Japanese). *Q. J. Seismol.*, 65, :123–134.

UMINO, N., KONO, T., OKADA, T., NAKAJIMA, J., MATSUZAWA, T., UCHIDA, N., et al. (2007). Relocation of the $M \sim 7$ Miyagi-oki Earthquakes in the 1930s: Seismic Slips of Asperities that Were Re-ruptured during the 1978 M7.4 Miyagi-oki Earthquake? *Zisin (Journal of the Seismological Society of Japan. 2nd Ser.)*, 59(4), 325–337. <https://doi.org/10.4294/zisin.59.325>

Umino, N., Kono, T., Okada, T., Nakajima, J., Matsuzawa, T., Uchida, N., et al. (2006). Revisiting the three $M \sim 7$ Miyagi-oki earthquakes in the 1930s: Possible seismogenic slip on asperities that were re-ruptured during the 1978 $M=7.4$ Miyagi-oki earthquake. *Earth, Planets and Space*, 58(12), 1587–1592. <https://doi.org/10.1186/BF03352666>

Vassiliou, M. S., & Kanamori, H. (1982). The energy release in earthquakes. *Bulletin of the Seismological Society of America*, 72(2), 371–387. Retrieved from <http://www.bssaonline.org/content/72/2/371.abstract>

Venkataraman, A., & Kanamori, H. (2004). Observational constraints on the fracture energy of subduction zone earthquakes. *Journal of Geophysical Research: Solid Earth*, 109(5). <https://doi.org/10.1029/2003JB002549>

- Waldhauser, F., & Ellsworth, W. L. (2000). A Double-Difference Earthquake Location Algorithm: Method and Application to the Northern Hayward Fault, California. *Bulletin of the Seismological Society of America*, *90*(6), 1353–1368. <https://doi.org/10.1785/0120000006>
- Wessel, P., & Smith, W. H. F. (1998). New, improved version of generic mapping tools released. *Eos, Transactions American Geophysical Union*, *79*(47), 579–579. <https://doi.org/10.1029/98EO00426>
- Wu, C., Koketsu, K., & Miyake, H. (2008). Source processes of the 1978 and 2005 Miyagi-oki, Japan earthquakes: Repeated rupture of asperities over successive large earthquakes. *Journal of Geophysical Research: Solid Earth*, *113*(8). <https://doi.org/10.1029/2007JB005189>
- Yaginuma, T., Okada, T., Yagi, Y., Matsuzawa, T., Umino, N., & Hasegawa, A. (2006). Coseismic slip distribution of the 2005 off Miyagi earthquake (M7.2) estimated by inversion of teleseismic and regional seismograms. *Earth, Planets and Space*, *58*(12), 1549–1554. <https://doi.org/10.1186/BF03352659>
- Yamanaka, Y., & Kikuchi, M. (2004). Asperity map along the subduction zone in northeastern Japan inferred from regional seismic data. *Journal of Geophysical Research: Solid Earth*, *109*(7). <https://doi.org/10.1029/2003JB002683>
- Yokota, Y., & Koketsu, K. (2015). A very long-term transient event preceding the 2011 Tohoku earthquake. *Nature Communications*, *6*. <https://doi.org/10.1038/ncomms6934>
- Yoshida, K., & Hasegawa, A. (2018). Hypocenter Migration and Seismicity Pattern Change in the Yamagata-Fukushima Border, NE Japan, Caused by Fluid Movement and Pore Pressure Variation. *Journal of Geophysical Research: Solid Earth*, *123*(6), 5000–5017. <https://doi.org/10.1029/2018JB015468>
- Yoshida, K., & Hasegawa, A. (2018). Sendai-Okura earthquake swarm induced by the 2011 Tohoku-Oki earthquake in the stress shadow of NE Japan: Detailed fault structure and hypocenter migration. *Tectonophysics*, *733*, 132–147. <https://doi.org/10.1016/j.tecto.2017.12.031>
- Yoshida, K., Uchida, N., Kubo, H., Takagi, R., & Xu, S. (2021). Prevalence of updip rupture propagation in interplate earthquakes along the Japan Trench. *Submitted to Earth and Planetary Science Letters*. <https://doi.org/https://www.essoar.org/doi/10.1002/essoar.10507292.1>